Tomographic Evidence for Localized Lithospheric Shear Along the Altyn Tagh Fault

Gérard Wittlinger, Paul Tapponnier, Georges Poupinet, Jiang Mei, Shi Danian, Georges Herquel, Frédéric Masson

Seismic tomography across the Altyn Tagh fault, at the north edge of the Tibetan Plateau, reveals a low *P*-wave velocity anomaly below the fault down to 140 kilometers. This anomaly probably reflects strike-slip shear in the lithosphere. Slip-partitioning may also induce a wedge of crust from the Tarim Basin to plunge into the mantle.

Convergence between India and Asia at a rate of 40 to 55 mm/year (*1*) has built much of the high topography north of the Ganges River in the last 55 million years (Fig. 1A). Despite recent evidence (*2–6*), the processes that have led to such uplift are debated. Compelling questions include where and how the convergence was absorbed, and what fraction of the convergence was taken up by thickening or extrusion (*7–10*). The extension at depth of fault zones or the fate of the lithospheric mantle is unknown. Answering such questions is essential to understand deformation mechanisms in Asia and other continents.

At the boundary between the Tibetan Plateau and the Tarim Basin, the Altyn Tagh fault (ATF) acts as a transfer zone, with thrusts at either end (Fig. 1A), forming a system that couples mountain building to strike-slip motion (*11*, *12*). Here we investigated whether strike-slip strain is limited to the crust (*13*) and whether the uppermost mantle thickens or founders beneath the northwestern edge of the Tibetan Plateau.

The ATF is the longest (~1800 km), active strike-slip fault of Asia (*11–14*). Its left-slip rate appears to be a few centimeters per year (*12*, *14*), and its total offset, several hundred kilometers (*4*, *8*). We performed seismic tomography between 87° and 92°E and 37° and 39°N (Fig. 1B), where the fault lies south of the Tibetan Plateau rim. Thrusting, ~90 km to the northwest, absorbs strike-perpendicular motion (*9*), uplifting the 4500-m-high, 600-km-long Altyn Tagh (Figs. 1B and 2A). The ATF thus juxtaposes the uplifted Precambrian basement of the Tarim Basin with the sediment fill of the Qaidam Basin. Coal-bearing Jurassic sandstones and ultramafic rocks are sheared along the fault zone. West of 90°E, a 15° restraining bend causes the additional rise of a narrow push-up range (the Akato Tagh, ~6000 m above sea level) bounded by thrusts (*14*) and sliced by the fault (Fig. 2A).

Thirty vertical one-component (1 Hz) seismic stations were installed near the Golmud-Ruoqiang road, which crosses the fault at Mangnai Zhen (~90.1°E, Fig. 1B), forming a 350-km-long profile oriented ~N112°E. To reduce difficulties inherent to single-profile tomography, we deployed short lateral extensions in the Tarim Basin (to B01) and southwest of Akato Tagh (to C05). From station A38 to the ATF (A25), the main profile follows the southwestern edge of the Qaidam Basin, ~40 km north of the Qiman Tagh. In this region, west-northwest–trending thrusts and broad anticlines folding 12 km of Jurassic to Pleistocene sediments (*15*) absorb part of the northeastward motion of the Tibetan Plateau relative to the Gobi Desert (*9*, *10*). Between stations A24 and A12, the profile first crosses a ~3000-m-high planation surface where gneisses and marbles are covered by thin Quaternary deposits. A steep, south-dipping fault then separates Tertiary red-beds from thick, folded Sinian limestones and schists that form the backbone of the Altyn Tagh which has its north flank bounded by an active thrust (Fig. 2A).

A total of 400 earthquakes were recorded by at least eight stations in 6 months (Fig. 1C). We selected earthquakes with the clearest *P*-wave arrival onsets, which reduced the data set to 3946 arrival times. The error associated with arrival time is 0.05 to 0.1 s (*16*). Inversion of *P*-wave residuals was performed with the ACH technique (*17*, *18*). The initial variance of the relative residuals, calculated with the starting model, was 0.148 s^2. After inversion, the variance was reduced by 92% to 0.011 s^2, equivalent to the a priori variance of the arrival times. The final model thus accounts for the observed residuals. The resolution matrix and tests (Fig. 3) show good resolution in the central part of the target volume (*19*).

In the southeastern part of the tomogram (Fig. 2B), negative velocity perturbations predominate at most depths, indicating a crust and mantle slower than reference beneath the southern Qaidam Basin and north edge of the high plateau (*16*). Northwest of the ATF, positive velocity perturbations appear at most depths, indicating faster than average crust and mantle, consistent with a cold and ancient lithosphere beneath the Tarim Basin.

A negative velocity perturbation extends into the crust and mantle beneath and along the ATF (Figs. 2B and 4). This latter perturbation is particularly clear because its boundaries involve the largest velocity contrasts, contrasts of up to 8% in the crust and 6% in the lithospheric mantle. Given the modest smearing (*19*), we estimate the width and depth of the ATF low-velocity anomaly to be ≤40 and ≤140 km, respectively.

Several processes may account for this relatively narrow and steep anomaly. Because slow *P*-wave velocities are observed in the upper crust, along Akato Tagh (Figs. 2B and 4A), water-filled cracks and chemical alteration may be involved. The shallowest part of the anomaly may thus be related to the 10- to 15-km-wide belt of faulted rocks, including asbestos-rich serpentinite bodies, observed along the fault (Fig. 2A). At greater depth, ductile shear (Figs. 2B and 4, B to E) is the most plausible source of the anomaly. The crust and mantle of adjacent regions, whether under the Qaidam Basin or the Altyn Tagh, show similarly high *P*-wave velocities (Fig. 2B), consistent with the western Qaidam lithosphere having been sliced off the Tarim block and displaced to the northeast.

A deep shear zone along the ATF low-velocity anomaly might resemble the metamorphic mylonite belt exhumed over a length of 900 km along the Red River fault in Yunnan and Vietnam (region 5 in Fig. 1) (*3*, *20*). This belt of steeply foliated, horizontally lineated gneisses, sheared for 20 million years at temperatures of 700° ± 100°C and depths of 15 to 25 km (*3*), is 20 km wide. With tomographic smearing, the source width of the ATF anomaly in the lower crust could be comparable. Both Tertiary fault zones are sinistral, plate-scale boundaries cutting across Precambrian crust (*3*). Both appear to have comparable slip rates [≥2 cm/year (*12*, *14*); 3 to 4 cm/year (*3*, *21*)] and finite offsets [≥500 km (*4*, *8*); 700 ± 200 km (*3*, *21*)]. Whereas sinistral motion along the Red River stopped 16 million years ago (*3*, *21*), the ATF is currently moving. With a plausible depth-averaged shear stress of 50 to 100 MPa (*22*), a present slip rate of ~2 cm/year would thus imply contemporaneous shear heating (*23*), and the corresponding temperature elevation might account for part of the velocity drop below 15 km along the ATF. We know of no local heat flow data, but by taking 40 mW m^{-2}

G. Wittlinger, G. Herquel, F. Masson, Institut de Physique du Globe de Strasbourg, Centre National de la Recherche Scientifique, Université Louis Pasteur, 5 rue R. Descartes 67084 Strasbourg, France. P. Tapponnier, Laboratoire de Tectonique, Institut de Physique du Globe de Paris, 4 Place Jussieu, 75205 Paris, France. G. Poupinet, Laboratoire de Géophysique Interne et Tectonophysique, Centre National de la Recherche Scientifique, Université Joseph Fourier, Boite Postale 53, 38041 Grenoble, France. J. Mei and S. Danian, Institute of Mineral Deposits, Chinese Academy of Geological Sciences, Baiwanzhuang Road, 100037 Beijing, China.

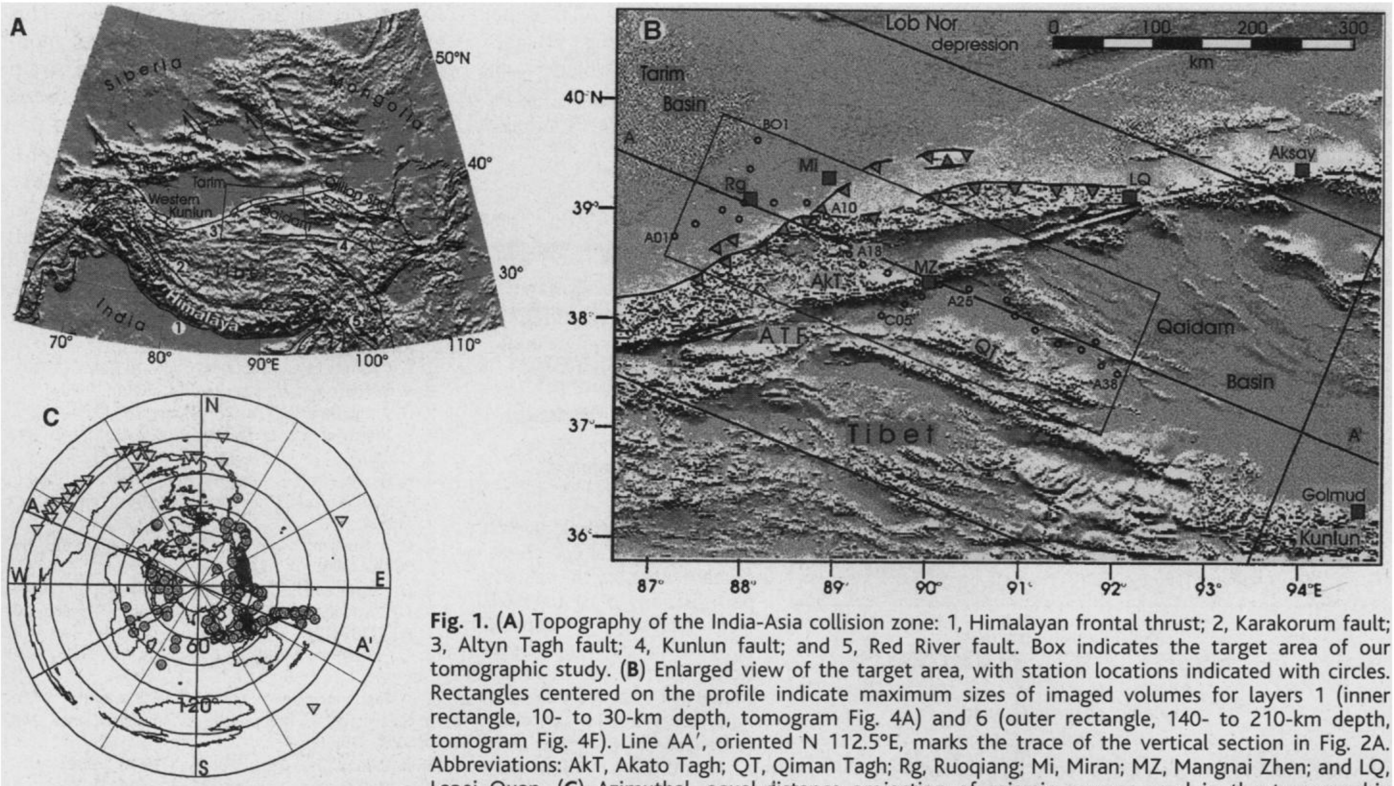

Fig. 1. (**A**) Topography of the India-Asia collision zone: 1, Himalayan frontal thrust; 2, Karakorum fault; 3, Altyn Tagh fault; 4, Kunlun fault; and 5, Red River fault. Box indicates the target area of our tomographic study. (**B**) Enlarged view of the target area, with station locations indicated with circles. Rectangles centered on the profile indicate maximum sizes of imaged volumes for layers 1 (inner rectangle, 10- to 30-km depth, tomogram Fig. 4A) and 6 (outer rectangle, 140- to 210-km depth, tomogram Fig. 4F). Line AA′, oriented N 112.5°E, marks the trace of the vertical section in Fig. 2A. Abbreviations: AkT, Akato Tagh; QT, Qiman Tagh; Rg, Ruoqiang; Mi, Miran; MZ, Mangnai Zhen; and LQ, Lapei Quan. (**C**) Azimuthal, equal-distance projection of seismic sources used in the tomographic inversion, located by NEIC (*28*). The map is centered at 38.382°N, 90.117°E, the reference point of the block model at the intersection between ATF and AA′. Epicentral distances and azimuths, evenly distributed relative to the observation network, are in degrees. Numerous sources located in the 45° sector centered on AA′ provide optimum ray crossing beneath the profile. Associated core phases for distances >120° (triangles) make the source distribution propitious for reliable inversion.

(*24*) as representative of the 2- to 2.5-billion-year-old crust crossed by our profile and using Karato's table (*25*), a fraction of the velocity decrease of 4% at a depth of 100 km would yield a 300°C temperature increase, hence a 30-km rise in the 900°C isotherm (Fig. 2B). That the anomaly vanishes at a depth of 140 to 150 km (*19*) may reflect the termination of the shear zone near the base of the moving lithospheric plates.

Part of the velocity drop below 50 km might also result from crustal underthrusting beneath the Altyn Tagh. The precipitous range front and the 80- to 90-m cumulative offset of Quaternary fans across the thrust south of Miran attest to fast shortening. On the tomogram (Fig. 2B), the thrust's emergence is marked by a footwall low-velocity anomaly that extends 20 km down, probably due to a wedge of Cenozoic sediments underthrust with the flexed foreland basement. A faint, 30°S dipping zone with slower velocity than the wedge of crust above may be traced farther to meet with the ATF anomaly at a depth of 80 km (Fig. 2). Shortening at a rate of 8 mm/year (*9, 10*) during the last 10 million years would have resulted in 80 km of underthrusting of the Tarim Basin crust, consistent with the southern edge of the ATF anomaly below 80 km dipping steeply southward to 150 km (Figs. 2 and 4). A slice of crust carried down by the plunging Tarim mantle and back-stopped by the Altyn Tagh shear zone might then contribute to the bottom half of the ATF anomaly. The schematic section of Fig. 2A resembles that inferred 1000 km westward across the western Kunlun (*4*). About 80 km of underthrusting of the Tarim lithosphere is also required to account for the isostatic gravity anomaly observed there (*26*). The high velocity perturbations underlying the Altyn Tagh down to 110 km (Fig. 2B) imply dense material beneath high relief, hence similar support by elastic flexure of the lithosphere. That underthrust-

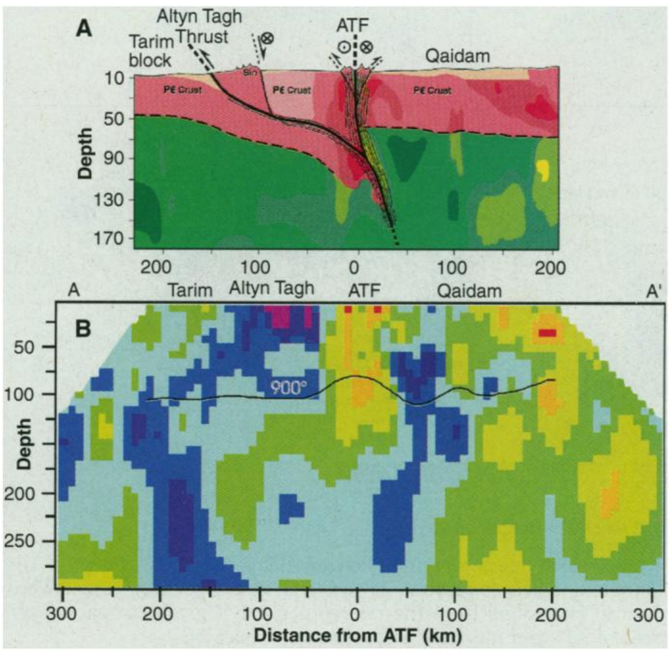

Fig. 2. (**A**) Section across the north edge of the Tibetan Plateau at 90°E. The simplified structure is consistent with the field geology and tomogram. Thick lines are boundary faults; dashed line, inferred Moho; and thin lines, foliation. Pale yellow corresponds to Cenozoic sediments and green and pink to mantle and crust, more yellow or red, respectively, where velocity is lower on the tomogram. (**B**) Tomographic vertical section along AA′, color scale as in Fig. 4. Solid line is computed 900°C isotherm. Depth in (A) and (B) is in kilometers.

ing of continental crust to a depth of 150 km can occur is attested to by the presence of ultra-high-pressure rocks containing coesite or diamonds in mountain ranges such as the Alps (*27*).

Our study suggests that the ATF is not restricted to the crust but controls, at lithospheric scale, the extrusion of large blocks—the Tibetan Plateau and the Qaidam Basin— as the Red River shear-zone did for Southeast Asia in the Oligocence and Miocene. This brings further support to mechanical models of continental collision in which strain localization in narrow zones between blocks governs the displacement field (*8–10*). Partitioning of slip occurs in the crust as the lithosphere of the Tarim Basin also plunges beneath the northwestern edge of the Tibetan Plateau. The Altyn Tagh fault thus behaves as an oblique plate boundary.

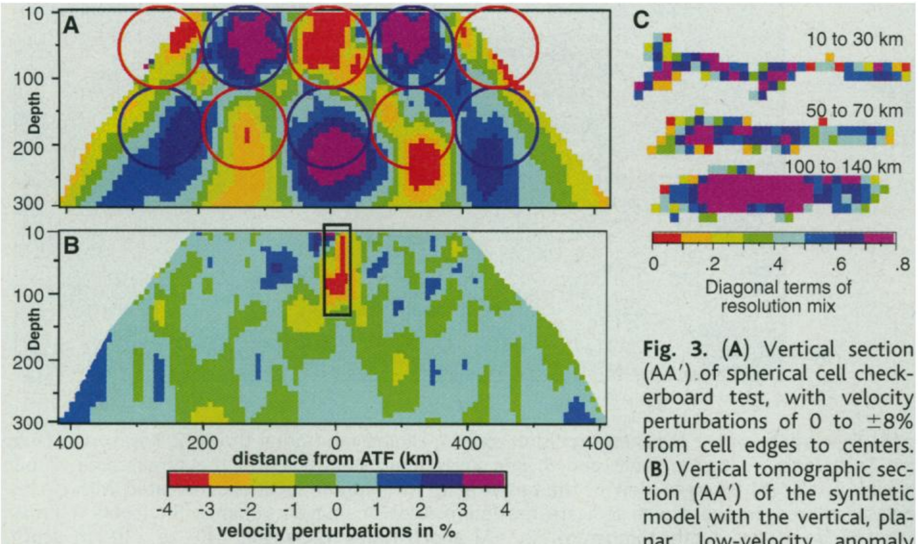

Fig. 3. (**A**) Vertical section (AA′) of spherical cell checkerboard test, with velocity perturbations of 0 to ±8% from cell edges to centers. (**B**) Vertical tomographic section (AA′) of the synthetic model with the vertical, planar, low-velocity anomaly (difference of 6%) that is 40 km wide and 140 km deep (solid rectangle) centered on ATF. Depth in (A) and (B) is in kilometers. (**C**) Diagonal terms of the resolution matrix for horizontal layers shown in Fig. 4, A, C, and E.

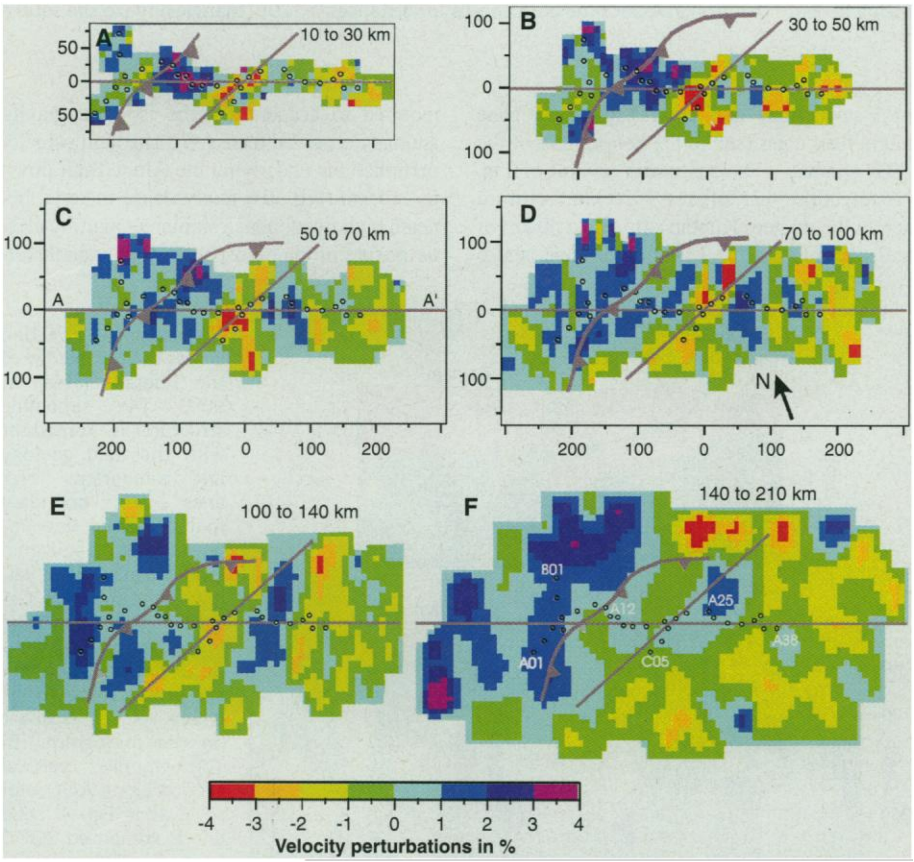

Fig. 4. (**A** to **F**) Fractional *P*-wave velocity perturbation in horizontal layers at various depths. The thin line is a trace of AA′. Purple and red correspond to fast and slow velocities, respectively. Distances along axes are given in kilometers from the reference point (Fig. 1). For each layer, projection of the surface traces of ATF and Altyn thrust (teethed) is indicated.

References and Notes

1. C. De Mets *et al.*, *Geophys. J. Int.* **101**, 425 (1990).
2. K. D. Nelson *et al.*, *Science* **274**, 1684 (1996).
3. H. P. Leloup *et al.*, *Tectonophysics* **251**, 3 (1995).
4. P. Matte *et al.*, *Earth Planet. Sci. Lett.* **142**, 311 (1996).
5. R. Armijo *et al.*, *J. Geophys. Res.* **94**, 2787 (1989).
6. P. Molnar and H. Lyon-Caen, *Geophys. J. Int.* **99**, 123 (1989).
7. G. A. Houseman and P. England, *J. Geophys. Res.* **86**, 3664 (1986).
8. G. Peltzer and P. Tapponnier, *ibid.* **93**, 15095 (1988).
9. J. P. Avouac and P. Tapponnier, *Geophys. Res. Lett.* **20**, 895 (1993).
10. G. Peltzer and F. Saucier, *J. Geophys. Res.* **101**, 27943 (1996).
11. P. Tapponnier and P. Molnar, *ibid.* **82**, 2905 (1977).
12. G. Peltzer, P. Tapponnier, R. Armijo, *Science* **246**, 1285 (1989).
13. B. C. Burchfiel *et al.*, *Geology* **17**, 478 (1989).
14. P. Molnar *et al.*, *Science* **235**, 299 (1987).
15. A. W. Bally *et al.*, *U.S. Geol. Surv. Open File Rep. 86* (1986).
16. G. Wittlinger *et al.*, *Earth Planet. Sci. Lett.* **139**, 263 (1996).
17. K. Aki, A. Christoffersson, E. Husebye, *J. Geophys. Res.* **82**, 277 (1977).
18. The ACH technique (*17*) involves partition of the target volume into layers (*7*) subdivided into blocks. Artifacts due to inappropriate initial model parametrization are minimized by averaging the results of five different inversions performed by shifting blocks horizontally by one half-block size in four orthogonal directions (*16*). The tomographic image is corrected for near-surface effects and sediment thickness by introducing a 10-km-thick surface layer with a cone below each station (*16*), for which a delay and velocity perturbation is computed. Because the cones do not overlap, the velocity perturbations are not smeared.
19. The resolution matrix (*16*) shows how the inverted model is related to the actual, unknown velocity model. Diagonal terms with values approaching 1 (in this study, >0.75 in the center of the target volume) testify to good resolution (Fig. 3C). Off-diagonal terms with values close to zero (in this study, <±0.1) indicate negligible smearing. Vertical cross sections (AA′, Fig. 1B) of a checkerboard test (Fig. 3A) and of a synthetic model with a single, vertical, planar low-velocity anomaly along the ATF (Fig. 3B) imply that anomalies of about ±1% are resolvable, and that smearing causes little depth or width increase in the central part of the tomogram.
20. P. Tapponnier *et al.*, *Nature* **343**, 431 (1990).
21. A. Briais *et al.*, *J. Geophys. Res.* **98**, 6299 (1993).
22. C. H. Scholz, *The Mechanics of Earthquakes and Faulting* (Univ. of Cambridge Press, Cambridge, 1990).
23. L. Fleitout and C. Froidevaux, *J. Struct. Geol.* **2**, 159 (1980).
24. J. C. Sclater *et al.*, *Rev. Geophys. Space Phys.* **18**, 269 (1981).
25. S. Karato, *Geophys. Res. Lett.* **20**, 1623 (1993).
26. H. Lyon-Caen and P. Molnar, *ibid.* **11**, 1251 (1984).
27. C. Chopin, *Contrib. Mineral. Petrol.* **86**, 107 (1984).
28. National Earthquake Information Center, *Preliminary Determination of Epicenters* (U.S. Department of the Interior/Geological Survey, Washington, DC, 1995).

29. This is contribution INSU-CNRS no. 116.

5 January 1998; accepted 11 August 1998